Assessing the importance of cation size in the tetragonal-cubic phase transition in lithium garnet electrolytes.

M. P. Stockham[1*], A. Griffiths[1], B. Dong[1], P.R. Slater[1*]

[1]School of Chemistry, University of Birmingham, Birmingham B15 2TT. UK

[2]School of Chemical Engineering, University of Birmingham, Birmingham B15 2TT. UK

Correspondence to

M. P. Stockham/P. R. Slater

School of Chemistry, University of Birmingham, Birmingham B15 2TT. UK

Abstract

Lithium garnets are promising solid-state electrolytes for next generation lithium-ion batteries. These materials have high ionic conductivity, a wide electrochemical window and stability with Li metal. However, lithium garnets have a maximum limit of 7 lithium atoms per formula unit (e.g. $La_3Zr_2Li_7O_{12}$), before the system transitions from a cubic to a tetragonal phase with poor ionic mobility. This arises from full occupation of the Li sites. Hence, the most conductive lithium garnets have Li between 6-6.55 Li per formula unit, which maintains the cubic symmetry and the disordered Li sub-lattice.

The tetragonal phase, however, forms the highly conducting cubic phase at higher temperatures, thought to arise from increased cell volume and entropic stabilisation permitting Li disorder. However, little work has been undertaken in understanding the controlling factors of this phase transition, which could enable enhanced dopant strategies to maintain room temperature cubic garnet at higher Li contents.

Here, a series of nine tetragonal garnets were synthesised and analysed via variable temperature XRD to understand the dependence of site substitution on the phase transition temperature. Interestingly the octahedral site cation radius was identified as the key parameter for the transition temperature with larger or smaller dopants altering the transition temperature noticeably. A site substitution was, however, found to make little difference irrespective of significant changes to cell volume.

Introduction

High-energy density, portable and safe energy storage remains one of the most prevalent issues in modern society. Lithium-ion batteries (LIB) are amongst the most promising options but are far from achieving their theoretical performance[1-3]. Maximal energy density of lithium batteries can only be achieved by use of Li metal anodes, which enable the highest theoretical capacity (3860 mA h g^{-1}) and the lowest electrochemical potential (−3.04 V vs. the standard hydrogen electrode) of all anode materials[1, 2]. However, current LIB electrolytes (usually $LiPF_6$ dissolved in a ethylene carbonate/dimethyl carbonate[22]) are incompatible with Li metal, present with safety concerns and an inability to accommodate high V cathode materials. Hence, electrolyte optimisation, or replacement, is paramount[1, 2, 4-8].

All solid-state batteries (ASSBs) are natural successors to current LIBs, as they could enable Li metal anodes, wider electrochemical windows and improved safety[9]. However, the development of a suitable solid-state electrolyte (SSE) has proved troublesome. To date many oxide and sulphide SSEs have been studied, but often have a high ionic conductivity or a wide electrochemical window, but rarely both[6, 9-15]. Finding a suitable SSE is, therefore, a key challenge to enable the next generation of energy storage[9].

Lithium garnets have emerged as contenders for use as an SSE, owing to a wide electrochemical window (0-6V vs Li/Li^+), chemical stability with Li metal and (in recent years) high ionic conductivity (> 0.1 mS cm^{-1})[16-40]. These materials, however, form a poorly conductive tetragonal phase at high Li content (as outlined below) and suffer from atmospheric H^+/Li^+ exchange (which ultimately forms insulating Li_2CO_3 passivating layers due to instability of the Li dopant in high concentrations)[41-44]. This is in addition to the common SSE problems of high interfacial resistance and time-consuming synthesis.

An ideal garnet has the formula; $A_3B_2X_3O_{12}$, where A, B and X are eight, six and four coordinated cation sites, respectively, which crystallise in a face-centred cubic structure (*e.g.* A = Mg, Fe, B = Al, Cr, Fe, and

X = Si, Fe, Al, Ga)[26, 45, 46]. This structure comprises BO_6 octahedra and XO_4 tetrahedra, arranged in a 3D framework wherein larger A cations occupy dodecahedral positions in the interstices[57,59]. Lithium ions fully occupy the tetrahedra 24d site, with 3 Li per formula unit (*pfu*). Alteration of A and B sites dopants, such as in $La_3Zr_2Li_7O_{12}$ (LLZO), enables up to 7 Li *pfu* (the upper maximum). However, at this point the system changes from a highly conductive cubic phase ($Ia\bar{3}d$ or $I4\bar{3}d$, Li content ~6.2-6.55 *pfu*), with vacant interstitial sites for ionic mobility, to a system whereby Li sites are fully occupied and have thus ordered (to reduce short Li-Li distances)[47-49]. This gives a reduction in symmetry from a cubic to a tetragonal cell ($I4_1/acd$) with ordered lithium occupying the tetrahedral (8a) and distorted octahedral (16f/32g) sites[32, 46-48, 50, 51].

However, these tetragonal Li garnets, such as $La_3Zr_2Li_7O_{12}$, $La_3Hf_2Li_7O_{12}$ and $Nd_3Zr_2Li_7O_{12}$, undergo a high temperature tetragonal-cubic phase transition (~700°C), believed to arise from increased unit cell size and entropy factors[52, 53]. It would therefore be of great interest if this transition temperature could be lowered to room temperature, thus forming a cubic Li_7 phase, which should further optimise the conductivity of Li garnets. This requires a greater understanding of the factors which influence the temperature of this phase transition, which is somewhat limited in the literature. Some studies initially thought this transition occurred ~100-200°C in LLZO but this was determined to arise from hydration, due to either the direct insertion of water molecules or through a H^+/Li^+ exchange mechanism[54]. Therefore, the characteristic, reversible tetragonal – cubic phase transition in LLZO is believed to be 620 - 650°C[13, 26, 54], while the smaller cell volume $La_3Sn_2Li_7O_{12}$ (LLSnO) exhibits a phase transition ~750 - 800°C[47, 51, 53]. This suggests that the cell volume is potentially key to dictating the phase transition.

Dong et al. investigated tetragonal garnets of the formula $La_3Zr_{2-x}Li_7Ce_xO_{12}$ ($0 \leq x \geq 0.75$) via XRD studies. This showed a reduction in tetragonality for these Li_7 garnets on Ce doping, attributed to the larger ionic radius of Ce^{4+}. This decreased the tetragonal-cubic transition temperature to 325°C compared to LLZO suggesting further that increased cell volume corresponds to lower transition temperatures[26].

However, density functional theory-based calculations by Chen et al., on tantalum doped systems (Ta-doped LLZO) and Li positioning changes in the phase transition, determined the thermodynamic stability of the tetragonal 16f site 'blocked' the formation of cubic LLZO at lower temperatures. Ta^{5+} doping was predicted to give octahedral site Li-ion vacancies which weakened the 'blocking' effect of the tetragonal (16f) sites, allowing for lithium-ion redistribution and thus, lowering the transition temperature[53]. These data indicate B site substitution could play an important role in the transition temperature, and that the direct relation to cell volume is perhaps too simplistic. Outside of these reports, work on the tetragonal to cubic phase transition is somewhat limited.

Herein nine tetragonal lithium garnets were synthesised; $A_3B_2Li_7O_{12}$ (A =La, Pr, Nd) (B = Zr, Hf), $La_3Zr_{1.75}Ce_{0.25}Li_7O_{12}$ and $LaSr_2B_2\ Li_7O_{12}$ (B = Nb, Ta). Both A and B site doping was undertaken to assess the relative importance of each site on the transition temperature. These materials were studied by variable temperature XRD analysis to ascertain if any new insights could be gained regarding the phase transition. Interestingly, we determine that, irrespective of A site substitution it is the B site which is the predominant factor in determining the phase transition temperature. It is shown that a direct relation solely to cell volume is too simplistic, rather it is suggested the sites which dictate the degree of tetragonality, which correspond to the framework polyhedra, are of higher importance than A site cations which reside within. Furthermore, the transition temperatures identified enabled regression analysis to predict the ideal octahedral B site radius for a room temperature stable cubic Li_7 phase.

Experimental

Solid – State Synthesis

$A_3B_2Li_7O_{12}$ (A = La, Pr, Nd) (B = Zr, Hf), $La_3Zr_{1.75}Ce_{0.25}Li_7O_{12}$ and $LaSr_2B_2Li_7O_{12}$ (B = Nb, Ta) were prepared via the solid-state route from stochiometric quantities of Li_2CO_3, Nd_2O_3, La_2O_3, Pr_6O_{11}, $SrCO_3$, ZrO_2, HfO_2, Nb_2O_5, CeO_2 Ta_2O_5. All were synthesised under air except for Pr based garnets which required treatment under 10% H_2 to ensure the formation of Pr^{3+}. A 20-40% mol excess of lithium was added to compensate for lithium loss during high temperature sintering. All tetragonal garnets were ball milled for 1 hr with ZrO_2 balls (500 rpm) with hexane. The powders were then pressed into 16 mm pellets and heated to 950-1100°C (6 -12 hours) at 5°C min^{-1}. Sr containing garnets were heated at 700°C (14hrs), 900°C (14 hrs) and 800°C (12hrs) (at 5°C min^{-1}), the latter of which also required a further 20% excess Li, illustrating challenges with the formation of these heavily Sr doped samples. Post sintering, pellets were sanded to remove any Al contamination from the Al crucible.

Characterisation

All samples were stored in an argon glove box to prevent proton-Li exchange in the garnet. Phase analysis was performed by X-ray diffraction (XRD) using a Bruker D8 diffractometer with Cu source from 15 – 80 2θ with a step size of 0.018°. Variable temperature measurements were conducted in a similar manner on a Bruker D8 instrument equipped with an Anton Parr heating stage from 50°C up to a maximum of 1000°C.

Rietveld Refinement

For each garnet synthesised, Rietveld refinements were performed in GSAS-II[55] using room temperature powder X-ray diffraction (XRD) patterns and variable temperature X-ray diffraction (VTXRD) patterns (50°C to 1000°C, 50°C increments). All structural models were obtained from ISCD[48, 49] and atoms altered where required to give an analogous crystal structure. For Ce-doped LLZO, fractional occupancies were set to the intended ratio.

Results and Discussion

X-ray diffraction

All nine Li_7 garnets were first analysed for phase purity at room temperature, and all were indexed on a tetragonal garnet cell ($I4_1/acd$). Variable temperature X-Ray diffraction (VTXRD) data were subsequently collected for these garnets up to 1000°C. This is beyond the common phase transition temperature (~700°C) but was required to reach the phase transition temperature for the Nb/Ta tetragonal phases. This caused some degradation for some systems; hence the complete reversal of the phase transition was not observed.

The tetragonal to cubic phase transition is readily noticeable in the VT-XRD patterns via the coalescence of the split peaks into sharp, singular peaks. Data were collected in 50°C increments (50°C – 1000°C), but were plotted every 100°C for clarity, see figure 1. Near the phase change temperature patterns were commonly biphasic (cubic and tetragonal phases present) and not used for structure refinements. Rietveld refinements were performed for all other XRD patterns with cell volume, cell parameters and A/B site bond lengths studied. An exemplar refinement (with tabulated data at each temperature) for LLZO is shown in figure 2 and table 1. Although these data were collected for all nine Li_7 phases, only LLZO is shown in detail, whereas table 2 shows the relevant data for the other eight phases only at room temperature and the transition temperature. Table 3 and 4 show bond lengths of A-O and B-O respectively.

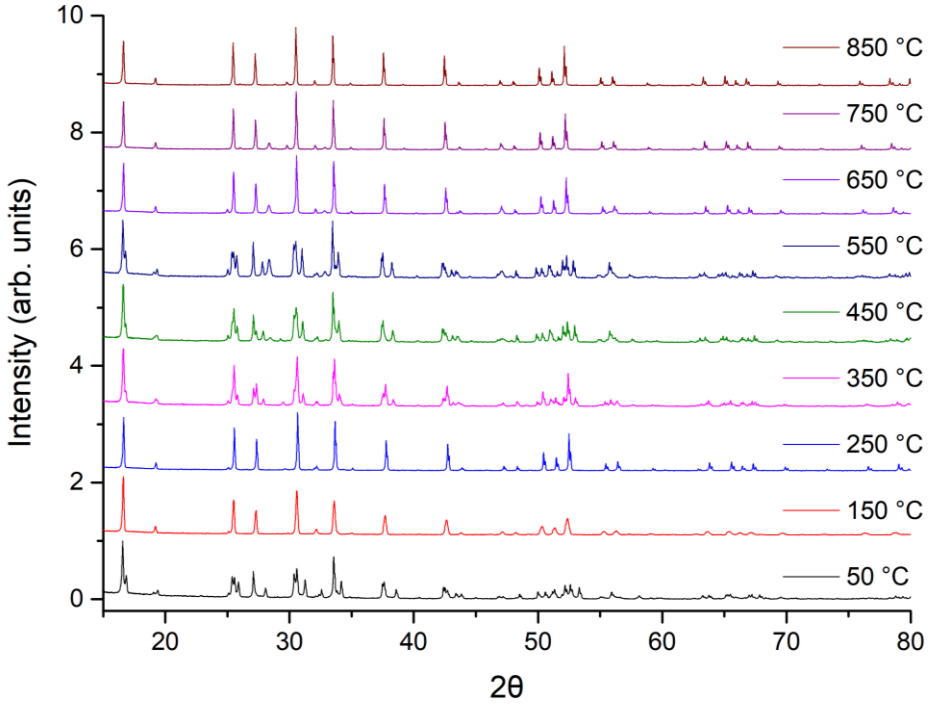

Figure 1 –$La_3Zr_2Li_7O_{12}$ stacked XRD patterns. Phase transitions are observed at ~150°C and ~650°C.

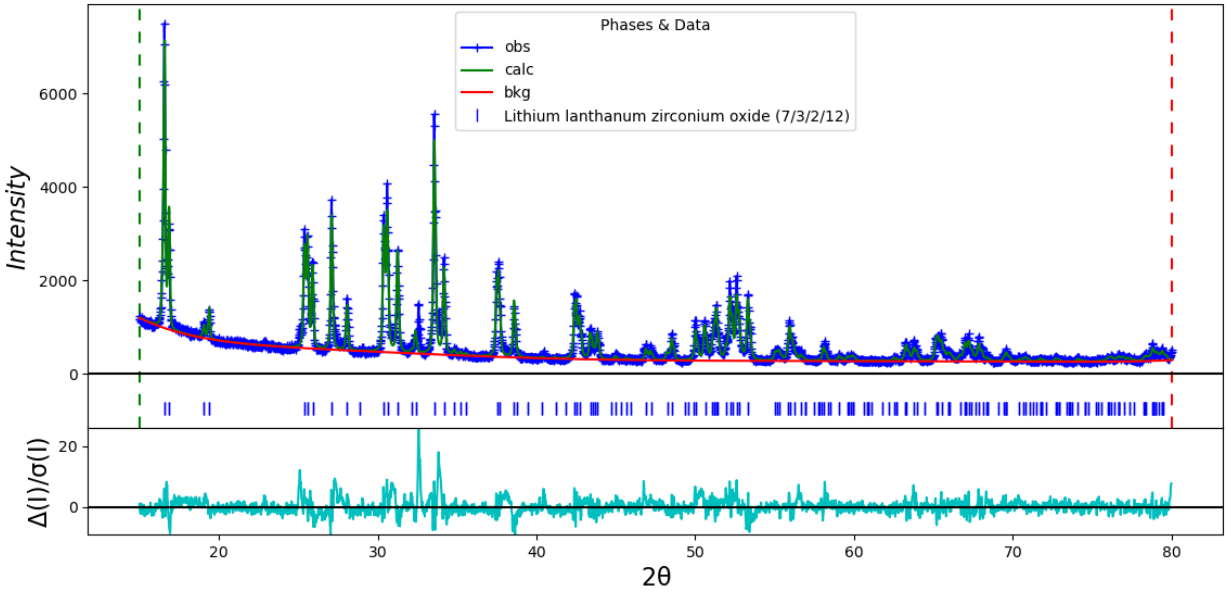

Figure 2 Observed, calculated and difference profiles for $La_3Zr_2Li_7O_{12}$ at 50°C, tetragonal (space group; $I4_1/acd$).

Temperature/°C	Unit cell parameters a	c	Degree of tetragonality	Cell volume/Å^3	Phase
50	13.1256(6)	12.6830(6)	0.966	2185.0(25)	Tetragonal
100	*Mixed phase. Transition occurring.*			-	-
150	13.0762(5)	-	-	2235.9(25)	Cubic
200	13.06019(15)	-2	-	2227.7(8)	Cubic
250	13.03577(17)	-	-	2215.2(9)	Cubic
300	*Mixed phase. Transition occurring.*			-	-
350	13.1257(22)	12.8038(21)	0.975	2205.9(10)	Tetragonal
400	13.1383(20)	12.8122(20)	0.975	2211.6(9)	Tetragonal
450	13.1775(7)	12.8206(7)	0.972	2226.3(3)	Tetragonal
500	13.1892(5)	12.8241(6)	0.973	2230.8(24)	Tetragonal
550	13.1942(5)	12.8510(5)	0.974	2237.2(22)	Tetragonal
600	13.1929(5)	12.8887(5)	0.977	2243.3(21)	Tetragonal
650	13.1057(29)	-	-	2251.0(15)	Cubic
700	13.1167(27)	-	-	2256.7(14)	Cubic
750	13.1275(25)	-	-	2262.3(13)	Cubic
800	13.1390(16)	-	-	2269.2(8)	Cubic
850	13.1522(15)	-	-	2275.3(8)	Cubic
900	13.1639(15)	-	-	2281.2(8)	Cubic
950	13.1756(19)	-	-	2287.3(10)	Cubic

Table 1 – Refinement data for $La_3Zr_2Li_7O_{12}$. Values in brackets represent standard errors. Degree of tetragonality is calculated as c/a.

Cell volume increased with temperature (table 1), as expected, across all the studied Li_7-garnets. This increase in cell volume coupled with the increasing importance of entropic stabilisation helps to promote disorder and drives the phase transition from tetragonal to cubic. Two distinct phase transitions were observed in all studied garnets, one ~100°C and a second at higher temperature. The phase transition at ~100°C was attributed to H^+/Li^+ exchange, as it was not possible to completely eliminate moisture. The second transition at much higher temperatures is attributed to the true tetragonal-cubic phase transition.

All $A_3Zr_2Li_7O_{12}$ (A = La, Pr, Nd) garnets had comparable phase transition temperatures (~600 - 650°C). This was a little surprising given the significant reduction in cell volume across the series from La -Pr-

Nd. In addition to little change in transition temperature there was also little change to the degree of tetragonality. Similarly little change was observed for the $A_3Hf_2Li_7O_{12}$ (A = La, Pr, Nd) series, although here the smaller Hf appears to have led to a small increase in the phase transition temperature to ~650 - 700°C. Therefore, it appears that doping on the A site has minimal effect on the phase transition, hence suggesting a direct relation to cell volume is too simplistic, as volume considerably reduces across these series of samples.

In contrast, a comparison of the Zr and Hf samples suggest an influence of B site doping, and that this effect requires only a very minimal difference in ionic radius between substituents. Further support for the effect of B site doping is shown by comparing further samples substituted on this site, such as the Ce-doped LLZO and $LaSr_2B_2Li_7O_{12}$ (B = Nb, Ta) phase. These showed clear differences in transition temperature, at ~325 - 425 °C and 800 - 900°C respectively (see table 2), with the lower transition temperature corresponding to the presence of larger cations in the B site. In line with the transition temperature changes, this corresponded to similar (Ce doped LLZO) and increased ($LaSr_2B_2Li_7O_{12,}$ B = Nb, Ta) degrees of tetragonality.

Overall the results were in contradiction with the common consensus; that the primary phase transition driving factor is the cell volume alone, as B site substitutions alter the cell volume considerably less than the A site substitutions yet give substantial differences in transition temperature, see figure 3[26, 53]. B site substitution in $LaSr_2B_2Li_7O_{12}$ also corresponds to larger increases in tetragonality. This indicates the B site plays a more key structural role in determining tetragonal distortion than the A site[26, 51]. This is logical given the garnet framework polyhedra of corner linked BO_6 and XO_4 units, as these sites would structurally define the cell more than the interstitial A site. Therefore, B site substitutions would have a greater chance of changing any structure-based transition temperature. This is supported by the results for $LaSr_2B_2Li_7O_{12}$ (B = Nb, Ta) and $La_3Sn_2Li_7O_{12}$ (tetragonality 0.956, transition temperature 750-800°C [51]) whereby large differences in tetragonality (compared to A site substitutions) correspond to higher transition temperatures. Hence, the cell

volume alone is not the ideal measure of transition temperature, rather the key numerical indicator could be considered the tetragonality which effectively mimics the thermodynamic energy barrier to overcome when transitioning from Li order to disorder.

However, only marginal changes in tetragonality are present for partial B site substitution with Ce-LLZO, yet significant changes in the transition are witnessed yet again. This further indicates the importance of the B site in dictating the temperature. In this respect, although only small changes in tetragonality are noted here, the work by Dong et al. (increasing Ce content up to 0.375) does indeed give noticeable changes in tetragonality (~0.980). This further suggests the B site is more responsible for the tetragonal distortion of the framework of the cell than the A site.

Analysis of bond distances shows the expected reduction in A-O bond lengths with the Zr/Hf samples, which correspond to decreased cell parameters arising from Ln contraction, see table 3. A-O distances are marginally smaller for the Hf based series which corresponds to a slightly higher transition temperature. The bond distances of $LaSr_2Ta_2Li_7O_{12}$, most directly comparable in terms of cell volume with $La_3Hf_2Li_7O_{12}$, show very similar A-O bond lengths despite the addition of Sr, yet show considerable reductions in B-O distances, further indicating the importance of B site substitution on the garnet structure.

Hence this suggests the degree of tetragonality is a more important indicator for the cell transition temperature, and that this is controlled more by the B site composition, as A site substituents have much reduced lattice parameters yet the degree of tetragonality remains similar, as do the transition temperatures.

Formula	Unit cell parameters		Degree of tetragonality	Cell volume (Å^3)	Transition temperature range (°C)
	a	*c*			
$La_3Zr_{1.75}Ce_{0.25}Li_7O_{12}$	13.1141(1)	12.7432(1)	0.972*	2191.6(10)	325 - 425
$La_3Zr_2Li_7O_{12}$	13.1242(6)	12.6791(6)	0.966	2183.90(26)	600 - 650
$Pr_3Zr_2Li_7O_{12}$	12.9783(3)	12.5653(3)	0.968	2116.5(11)	600 - 650
$Nd_3Zr_2\ Li_7O_{12}$	12.9222(7)	12.5501(7)	0.971	2095.64(29)	600 - 650
$La_3Hf_2Li_7O_{12}$	13.1049(21)	12.6474(19)	0.965	2172.0(10)	650 - 700
$Pr_3Hf_2Li_7O_{12}$	12.9700(10)	12.5417(9)	0.967	2109.8(5)	650 - 700
$Nd_3Hf_2Li_7O_{12}$	12.9118(7)	12.9118(7)	0.969	2085.7(28)	650 - 700
$LaSr_2Nb_2Li_7O_{12}$	13.0752(16)	12.5091(15)	0.957	2138.6(7)	800 - 900
$LaSr_2Ta_2Li_7O_{12}$	13.1431(8)	12.5433(8)	0.954	2166.8(3)	800 - 900

Table 2 – Refinement data for all nine Li_7-garnet systems studied. Values within brackets refer to standard deviations. (Note lattice parameters and tetragonality are all based on room temperature XRD data.)

Formula	A(1) - O bond length/Å (average)	A(2) - O bond length/Å (average)	Transition temperature/°C
$La_3Zr_{1.75}Ce_{0.2}\ Li_{75}O_{12}$	2.628	2.604	325 - 425
$La_3Zr_2Li_7O_{12}$	2.587	2.543	600 - 650
$Pr_3Zr_2Li_7O_{12}$	2.535	2.506	600 - 650
$Nd_3Zr_2Li_7O_{12}$	2.527	2.497	600 - 650
$La_3Hf_2Li_7O_{12}$	2.583	2.539	650 - 700
$Pr_3Hf_2Li_7O_{12}$	2.533	2.503	650 - 700
$Nd_3Hf_2Li_7O_{12}$	2.523	2.493	650 - 700
$LaSr_2Nb_2Li_7O_{12}$	2.570	2.526	800 - 900
$LaSr_2Ta_2Li_7O_{12}$	2.581	2.537	800 - 900

Table 3– A site bond length data for all nine Li_7-garnet systems studied. Values within brackets refer to standard deviations.

(Note lattice parameters and tetragonality all based on room temperature data.)

Formula	B(1) - O bond length/Å (average)	Transition temperature (°C)
$La_3Zr_{1.75}Ce_{0.25}\ Li_7O_{12}$	2.117	325 - 425
$La_3Zr_2Li_7O_{12}$	2.113	600 - 650
$Pr_3Zr_2Li_7O_{12}$	2.105	600 - 650
$Nd_3Zr_2Li_7O_{12}$	2.098	600 - 650
$La_3Hf_2Li_7O_{12}$	2.109	650 - 700
$Pr_3Hf_2Li_7O_{12}$	2.102	650 - 700
$Nd_3Hf_2Li_7O_{12}$	2.094	650 - 700
$LaSr_2Nb_2Li_7O_{12}$	2.107	800 - 900
$LaSr_2Ta_2Li_7O_{12}$	2.098	800 - 900

Table 4 – B site bond length data for all nine Li_7-garnet systems studied. Values within brackets refer to standard deviations.

(Note lattice parameters and tetragonality all based on room temperature data.)

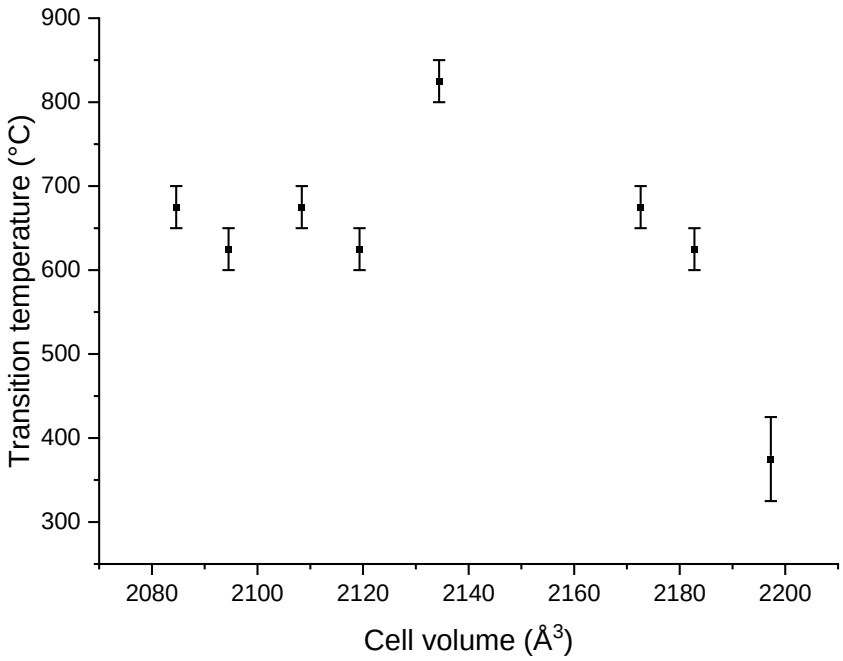

Figure 3 – Room temperature cell volume vs transition temperature range, illustrating no clear trend.

Garnet formula	Octahedral site ionic radii/Å	Transition temperature range/°C
$La_3Zr_{1.75}Ce_{0.25}Li_7O_{12}$	0.74	325 – 425
$La_3Zr_2Li_7O_{12}$	0.72	600 - 650
$Pr_3Zr_2Li_7O_{12}$	0.72	600 - 650
$Nd_3Zr_2Li_7O_{12}$	0.72	600 - 650
$La_3Hf_2Li_7O_{12}$	0.71	650 - 700
$Pr_3Hf_2Li_7O_{12}$	0.71	650 - 700
$Nd_3Hf_2Li_7O_{12}$	0.71	650 - 700
$LaSr_2Nb_2Li_7O_{12}$	0.64	800 - 900
$LaSr_2Ta_2Li_7O_{12}$	0.64	800 - 900

Table 5 – Summary of octahedral site ionic radii for the series of Li_7-garnets studied. (For the Ce-doped garnet, where dual doping on the octahedral site is observed, a weight averaged value is used for the radius)

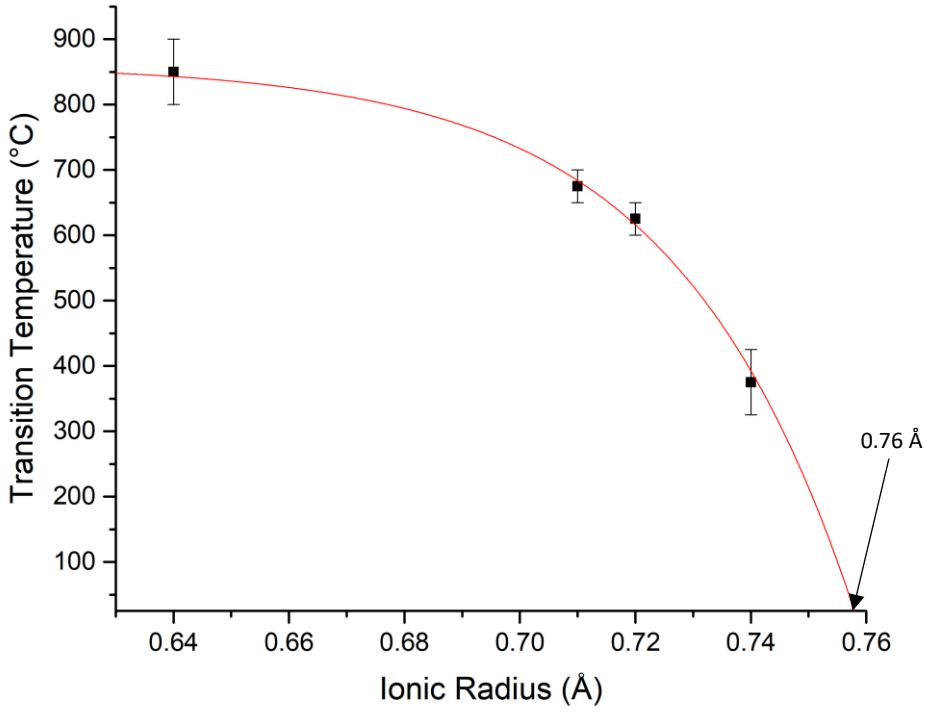

Figure 4- Octahedral site ion radii vs transition temperature range, several ionic radii are similar and thus superimposed. The data was fit using an exponential function as per Equation 1; data suggests a room temperature cubic phase would require an average octahedral site ionic radius of 0.76 Å.

The temperature differential becomes even clearer when octahedral site ion radii vs the transition temperature range are shown, see figure 4. This shows considerable difference in B site substituents compared to the A site (most A site doping results are superimposed over each other). Figure 4 shows a clear mathematical relationship as per equation 1, perhaps adding further evidence to octahedral site ion size being a key determining factor. Regression on figure 4 yields an extrapolated octahedral site radius which could enable room temperature (20°C) stable cubic lithium garnet phases with the average B cation site size at approximately 0.76 Å.

$$y = y_0 + Ae^{R_0 x}$$

Equation 1. Exponential function with rate constant parameter which was used for fitting the data in figure 4.

As such, attempts to increase Ce content beyond the 0.25 reported by Dong et al. were made, via employing dry room facilities. However, this led to Ce based impurities (see figure 5), in addition to tetragonal LLZO, similar to the reports in the work[26]. As employing larger 4+ ions than Ce is not feasible, co-doping strategies (such as Y/Nb or Sc/Nb) need to be considered to reach the octahedral radius of 0.76 Å. For example, a garnet with formula of $La_3YNbLi_7O_{12}$ yields an average octahedral site radius of 0.77 Å[72]. This was attempted via the standard solid state route. While, this did indeed yield a cubic phase, large Nb, Y and La oxide-based impurities were present, see figure 6.

In terms of future work, a further factor that could be examined to alter the transition temperature is the oxygen site. This determination of the phase transition temperature via O site substitution has yet to be explored, although has been considered as potential room temperature cubic phase stabilisation prior[107]. However, assessment via Cl or F substitution with O on the phase transition temperature is complex, as high temperatures can easily remove the halogen dopant forming more thermodynamically stable by-products. Further correlative evidence could be found by investigating the transition temperature by changing the XO_4 sites, this may yield further confirmation of the controlling factors, but would not necessarily aid in cubic Li_7 phase formation

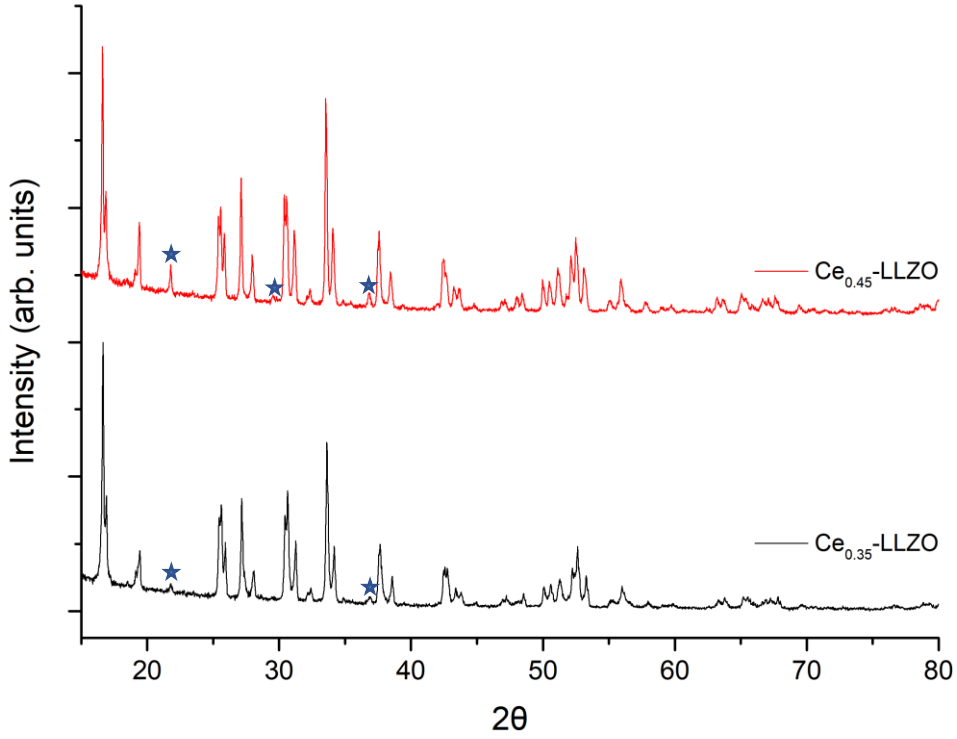

Figure 5. PXRD patterns for $La_3Zr_{2-x}Ce_xLi_7O_{12}$ (x = 0.35, 0.45) attempted via the standard solid state route, leading to impurities for higher Ce levels. Blue stars mark the impurities.

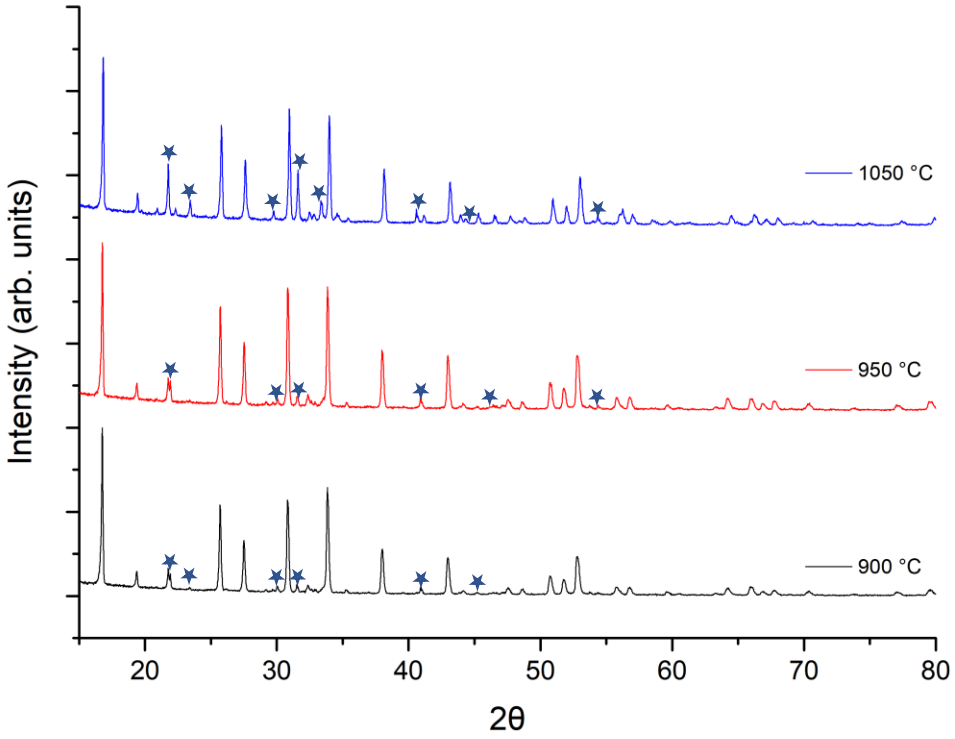

Figure 6. PXRD patterns for $La_3YNbLi_7O_{12}$ attempted via the standard solid state route between 900-1050°C showing a cubic garnet phase with additional impurities. Blue stars mark the impurities.

Conclusions

To conclude, it is suggested that the primary factor in the determination of the temperature of the tetragonal – cubic phase transition in the Li_7-garnet systems is the B site, which is suspected to arise from the fact that this cation helps to dictate the garnet framework structure, in contrast to the A site, which occupies the cavities within the framework of corner linked octahedra and tetrahedra. This is illustrated by the fact that octahedral site doping showed significant changes to the transition temperature, whereas negligible changes were observed for A site doping. Changes can be correlated to the degree of tetragonality which appears to be dependent on B site dopant size, rather than the cell volume. This work shows that as the degree of tetragonality of the garnet increases, the transition temperature increases too. Therefore, it is hypothesized that the octahedral site is instrumental in determining the tetragonality of the phase, and hence doping at this site with larger cations is the best method in lowering the transition temperature. A similar affect could also be the case for doping in the XO_4 tetrahedra (which are also part of the garnet framework) and may help to explain the stability of Li site doping by Ga/Al and subsequent formation of the cubic phase.

Further work by neutron diffraction is required to clarify this relationship more accurately, however, once this phase transition is fully understood, it is hoped that Li_7 phases could be cubic at room temperature, thus enabling a higher conductivity SSE.

Acknowledgements

We would like to thank the University of Birmingham for the studentship funding of Mark Stockham.

References

1. M. Armand and J. M. Tarascon, *Nature*, 2008, **451**, 652.
2. J. M. Tarascon and M. Armand, *Nature*, 2001, **414**, 359.
3. Y. Zhu, X. He and Y. Mo, *ACS Appl. Mater. Interfaces*, 2015, **7**, 23685-23693.
4. C.-X. Zu and H. Li, *Energy & Environmental Science*, 2011, **4**, 2614-2624.
5. V. A. Agubra and J. W. Fergus, *Journal of Power Sources*, 2014, **268**, 153-162.
6. J. G. Kim, B. Son, S. Mukherjee, N. Schuppert, A. Bates, O. Kwon, M. J. Choi, H. Y. Chung and S. Park, *Journal of Power Sources*, 2015, **282**, 299-322.
7. X. Xiong, Q. Zhou, Y. Zhu, Y. Chen, L. Fu, L. Liu, N. Yu, Y. Wu and T. van Ree, *Energy & Fuels*, 2020, **34**, 10503-10512.
8. V. Etacheri, R. Marom, R. Elazari, G. Salitra and D. Aurbach, *Energy & Environmental Science*, 2011, **4**, 3243-3262.
9. J. Li, C. Ma, M. Chi, C. Liang and N. J. Dudney, *Advanced Energy Materials*, 2015, **5**, 1401408.
10. B. Dong, J. Yan, B. Walkley, K. K. Inglis, F. Blanc, S. Hull and A. R. West, *Solid State Ion.*, 2018, **327**, 64-70.
11. V. Thangadurai, S. Narayanan and D. Pinzaru, *Chemical Society Reviews*, 2014, **43**, 4714-4727.
12. W. D. Richards, L. J. Miara, Y. Wang, J. C. Kim and G. Ceder, *Chemistry of Materials*, 2016, **28**, 266-273.
13. S. Ramakumar, C. Deviannapoorani, L. Dhivya, L. S. Shankar and R. Murugan, *Progress in Materials Science*, 2017, **88**, 325-411.
14. Q. Zhao, S. Stalin, C.-Z. Zhao and L. A. Archer, *Nature Reviews Materials*, 2020, **5**, 229-252.
15. C. Li, Z.-y. Wang, Z.-j. He, Y.-j. Li, J. Mao, K.-h. Dai, C. Yan and J.-c. Zheng, *Sustainable Materials and Technologies*, 2021, **29**, e00297.
16. C. Bernuy-Lopez, W. Manalastas, J. M. Lopez del Amo, A. Aguadero, F. Aguesse and J. A. Kilner, *Chemistry of Materials*, 2014, **26**, 3610-3617.
17. B. Dong, L. L. Driscoll, M. P. Stockham, E. Kendrick and P. R. Slater, *Solid State Ion.*, 2020, **350**, 115317.
18. B. Dong, M. P. Stockham, P. A. Chater and P. R. Slater, *Dalton Transactions*, 2020, **49**, 11727-11735.
19. M. P. Stockham, B. Dong, Y. Ding, Y. Li and P. R. Slater, *Dalton Transactions*, 2020, DOI: 10.1039/D0DT01497D.
20. M. P. Stockham, B. Dong, M. S. James, Y. Li, Y. Ding and P. R. Slater, *Dalton Transactions*, 2021, **50**, 2364-2374.
21. J. L. Allen, J. Wolfenstine, E. Rangasamy and J. Sakamoto, *Journal of Power Sources*, 2012, **206**, 315-319.
22. S.-W. Baek, J.-M. Lee, T. Y. Kim, M.-S. Song and Y. Park, *Journal of Power Sources*, 2014, **249**, 197-206.
23. H. Buschmann, J. Dölle, S. Berendts, A. Kuhn, P. Bottke, M. Wilkening, P. Heitjans, A. Senyshyn, H. Ehrenberg, A. Lotnyk, V. Duppel, L. Kienle and J. Janek, *Physical Chemistry Chemical Physics*, 2011, **13**, 19378-19392.
24. Y. Chen, E. Rangasamy, C. Liang and K. An, *Chemistry of Materials*, 2015, **27**, 5491-5494.
25. E. J. Cheng, A. Sharafi and J. Sakamoto, *Electrochimica Acta*, 2017, **223**, 85-91.
26. B. Dong, S. R. Yeandel, P. Goddard and P. R. Slater, *Chemistry of Materials*, 2020, **32**, 215-223.
27. K. Fu, Y. Gong, B. Liu, Y. Zhu, S. Xu, Y. Yao, W. Luo, C. Wang, S. Lacey, J. Dai, Y. Chen, Y. Mo, E. Wachsman and L. Hu, *Science Advances*, 2017, **3**, e1601659.
28. C. Galven, J.-L. Fourquet, M.-P. Crosnier-Lopez and F. Le Berre, *Chemistry of Materials*, 2011, **23**, 1892-1900.
29. Y. X. Gao, X. P. Wang, W. G. Wang and Q. F. Fang, *Solid State Ion.*, 2010, **181**, 33-36.
30. M. Huang, A. Dumon and C.-W. Nan, *Electrochemistry Communications*, 2012, **21**, 62-64.
31. H. M. Kasper, *Inorganic Chemistry*, 1969, **8**, 1000-1002.

32. R. Murugan, V. Thangadurai and W. Weppner, *Angewandte Chemie International Edition*, 2007, **46**, 7778-7781.
33. S. Narayanan, F. Ramezanipour and V. Thangadurai, *J. Phys. Chem. C*, 2012, **116**, 20154-20162.
34. M. P. O'Callaghan, D. R. Lynham, E. J. Cussen and G. Z. Chen, *Chemistry of Materials*, 2006, **18**, 4681-4689.
35. J. Percival, D. Apperley and P. R. Slater, *Solid State Ion.*, 2008, **179**, 1693-1696.
36. J. Percival, E. Kendrick and P. R. Slater, *Solid State Ion.*, 2008, **179**, 1666-1669.
37. F. M. Pesci, A. Bertei, R. H. Brugge, S. P. Emge, A. K. O. Hekselman, L. E. Marbella, C. P. Grey and A. Aguadero, *ACS Appl. Mater. Interfaces*, 2020, **12**, 32806-32816.
38. E. Rangasamy, J. Wolfenstine and J. Sakamoto, *Solid State Ion.*, 2012, **206**, 28-32.
39. V. Thangadurai, H. Kaack and W. J. F. Weppner, *Journal of the American Ceramic Society*, 2004, **86**, 437-440.
40. R. Wagner, G. J. Redhammer, D. Rettenwander, A. Senyshyn, W. Schmidt, M. Wilkening and G. Amthauer, *Chemistry of Materials*, 2016, **28**, 1861-1871.
41. G. V. Alexander, S. Patra, S. V. Sobhan Raj, M. K. Sugumar, M. M. Ud Din and R. Murugan, *Journal of Power Sources*, 2018, **396**, 764-773.
42. R. H. Brugge, F. M. Pesci, A. Cavallaro, C. Sole, M. A. Isaacs, G. Kerherve, R. S. Weatherup and A. Aguadero, *Journal of Materials Chemistry A*, 2020, **8**, 14265-14276.
43. L. Cheng, E. J. Crumlin, W. Chen, R. Qiao, H. Hou, S. Franz Lux, V. Zorba, R. Russo, R. Kostecki, Z. Liu, K. Persson, W. Yang, J. Cabana, T. Richardson, G. Chen and M. Doeff, *Physical Chemistry Chemical Physics*, 2014, **16**, 18294-18300.
44. F. Flatscher, M. Philipp, S. Ganschow, H. M. R. Wilkening and D. Rettenwander, *Journal of Materials Chemistry A*, 2020, **8**, 15782-15788.
45. A. F. Wells, *Structural inorganic chemistry*, Clarendon Press, 1984.
46. E. J. Cussen and T. W. S. Yip, *Journal of Solid State Chemistry*, 2007, **180**, 1832-1839.
47. C. A. Geiger, E. Alekseev, B. Lazic, M. Fisch, T. Armbruster, R. Langner, M. Fechtelkord, N. Kim, T. Pettke and W. Weppner, *Inorganic Chemistry*, 2011, **50**, 1089-1097.
48. J. Awaka, N. Kijima, H. Hayakawa and J. Akimoto, *Journal of Solid State Chemistry*, 2009, **182**, 2046-2052.
49. J. Awaka, N. Kijima, K. Kataoka, H. Hayakawa, K.-i. Ohshima and J. Akimoto, *Journal of Solid State Chemistry*, 2010, **183**, 180-185.
50. E. J. Cussen, *Chemical Communications*, 2006, DOI: 10.1039/B514640B, 412-413.
51. J. Percival, E. Kendrick, R. I. Smith and P. R. Slater, *Dalton Transactions*, 2009, DOI: 10.1039/b907331k, 5177-5181.
52. N. Bernstein, M. D. Johannes and K. Hoang, *Physical Review Letters*, 2012, **109**, 205702.
53. F. Chen, J. Li, Z. Huang, Y. Yang, Q. Shen and L. Zhang, *The Journal of Physical Chemistry C*, 2018, **122**, 1963-1972.
54. G. Larraz, A. Orera and M. L. Sanjuán, *Journal of Materials Chemistry A*, 2013, **1**, 11419-11428.
55. B. Toby and R. Dreele, *Journal of Applied Crystallography*, 2013, **46**, 544-549.